Correlation measurements of individual microwave photons emitted from a symmetric cavity

D. Bozyigit, C. Lang, L. Steffen, J. M. Fink, C. Eichler, M. Baur, R. Bianchetti, P. J. Leek, S. Filipp and A. Wallraff

Department of Physics, ETH Zürich, CH-8093, Zürich, Switzerland.

E-mail: `andreas.wallraff@phys.ethz.ch`

M. P. da Silva, A. Blais

Département de Physique, Université de Sherbrooke, Sherbrooke, Québec, J1K 2R1 Canada.

Abstract. Superconducting circuits have been successfully established as systems to prepare and investigate microwave light fields at the quantum level. In contrast to optical experiments where light is detected using photon counters, microwaves are usually measured with well developed linear amplifiers. This makes measurements of correlation functions - one of the important tools in optics - harder to achieve because they traditionally rely on photon counters and beam splitters. Here, we demonstrate a system where we can prepare on demand single microwave photons in a cavity and detect them at the two outputs of the cavity using linear amplifiers. Together with efficient data processing, this allows us to measure different observables of the cavity photons, including the first-order correlation function. Using these techniques we demonstrate cooling of a thermal background field in the cavity.

Correlation function measurements are one of the most important tools in quantum optics to investigate the properties of radiation [1]. In such measurements one observes the ability of light to interfere with itself as quantified by first and second-order correlation functions [2, 3]. The radiation to be characterized is usually passed through a beam splitter and subsequently its interference is observed in Mach-Zehnder interferometer or Hanbury Brown-Twiss type setups [4]. At optical frequencies the light is commonly detected using readily available photon counters. In the microwave regime, however, no efficient photon counters exist to date, as photons at these much lower frequencies carry an energy that is orders of magnitude less than at optical frequencies. Instead, most experiments rely on a detection of electric field quadratures using linear amplifiers and oscilloscopes. Although linear microwave amplifiers can be used to reliably detect fields on the single photon level using averaging techniques [5] they necessarily add noise to the signal [6]. Despite the lack of photon detectors, it was shown recently [7] that correlation functions are also accessible in electric field quadratures detection schemes.

In the microwave regime beam splitters are typically implemented as so called hybrids [8]. Similar to the optical case, these are devices that rely on the interference of light propagating along different paths. Therefore, their size is determined by the radiation wavelength which is on the order of 1 cm at microwave frequencies. This makes an on-chip beam splitter a sizable device, which is not yet commonly used in quantum microwave experimental setups. While first realizations in superconducting microwave electronics are being demonstrated [9–12] they still
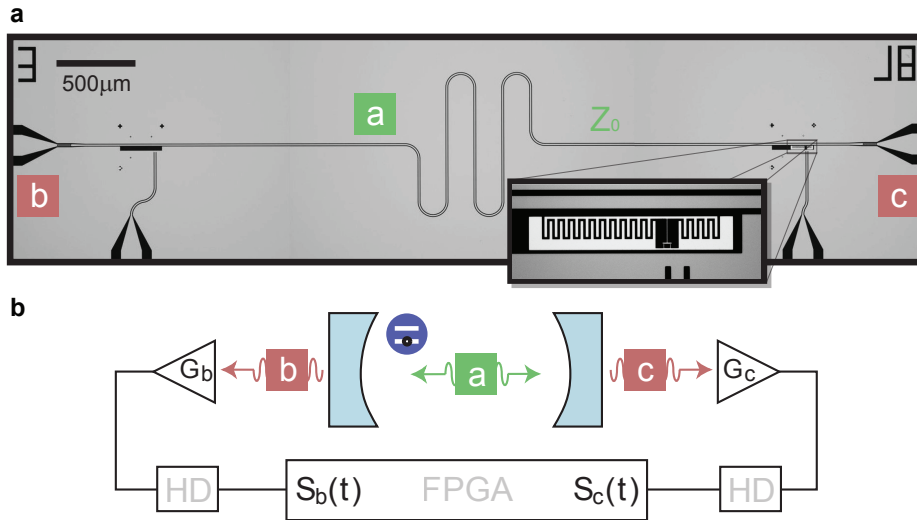
Figure 1. Experimental setup. a, Microscope image of our sample with superconducting microwave transmission line resonator and transmon qubit in the resonator gap (see inset). Two output lines are coupled symmetrically on the left and right. **b**, Schematic of the experimental setup. A two-level system emits a photon into the cavity mode a defined by two mirrors. Linear amplifiers with gain $G_{b,c}$ couple symmetrically to the cavity outputs amplifying the radiation in output modes b and c. Heterodyne detectors (HD) extract both quadratures of the output fields and feed results to field programmable gate array (FPGA) based digital correlation electronics.

require additional effort in the fabrication process.

Here, we present measurements of the first-order correlation function of single microwave photons. We explore an architecture which features two channel detection without employing a beam splitter by using the two outputs of a symmetric microwave cavity. Furthermore we demonstrate that by recording the time series of the detected quadrature signal – instead of its time average – and using efficient digital signal processing, we can extract the first-order correlation function of radiation generated by microwave frequency emitters. Interestingly they allow us to observe the cooling of a thermal background field in the resonator through the interaction with the qubit. The measurements presented here were performed before samples with integrated beam splitters were available to us. Nevertheless, they demonstrate the feasibility of our detection technique. Based on these results we have performed measurements of the second-order correlation function in an optimized setup which allows the observation of strictly quantum mechanical effects such as single photon antibunching [12].

For our experiments we have realized a superconducting electronic circuit (Fig. 1a), similar to the one presented in [5]. In our circuit, we coherently and controllably couple a single qubit to a high quality resonator to create an individual photon on demand. The superconducting transmon qubit [13] used in this experiment is characterized by its maximum Josephson energy $E_{J,max} \approx 14.4\,\text{GHz}$, its charging energy $E_C \approx 500\,\text{MHz}$ and its energy relaxation and dephasing times in excess of a few hundred nanoseconds. The transition frequency of the qubit is flux tunable using both a quasi-static magnetic field generated with a miniature coil and an on chip transmission line to generate nanosecond time scale flux pulses. By integrating our qubit into a superconducting coplanar transmission line resonator of frequency $\nu_r = 6.433\,\text{GHz}$ and quality factor $Q = 2060$ we couple it strongly to a single mode a of the radiation field stored in the resonator. This approach is known as circuit quantum electrodynamics [14] and allows to study
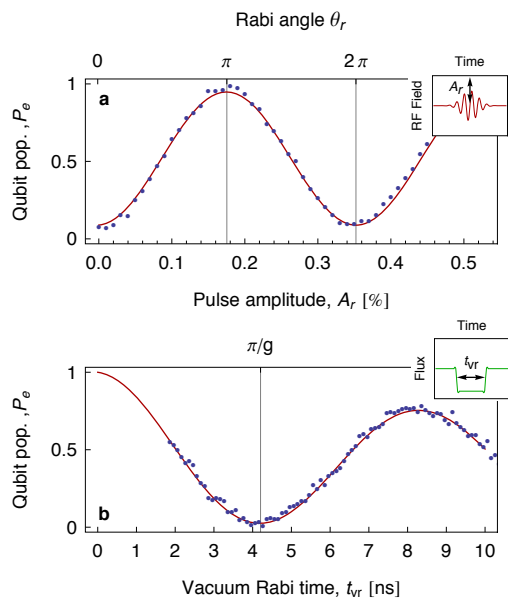
Figure 2. Control of qubit state and qubit/resonator interaction. a, Qubit excited state population P_e versus Rabi pulse amplitude A_r. The Rabi rotation angle θ_r is indicated on the top axis. The used pulse shape is shown in the inset. **b**, P_e versus qubit-resonator interaction time t_{vr} with the used flux pulse shape in the inset. Note that the interaction time can experimentally not be made shorter than 1.9 ns due to the finite rise time of the pulses. Dots are data and lines are fits to an analytic model of an exponentially decaying sinusoid.

in exquisite detail the interaction of quantum two-level systems with quantized radiation fields.

In this system we implement a single photon source using the following procedure. Applying a phase controlled truncated Gaussian microwave pulse of variable amplitude A_r and total duration $t_r = 18$ ns to the qubit biased at a transition frequency of $\nu_q = 6.933$ GHz, we prepare a superposition state $|\psi_q\rangle = \alpha|g\rangle + \beta|e\rangle$ between the qubit ground $|g\rangle$ and excited states $|e\rangle$. The superposition is characterized by the two complex probability amplitudes $\alpha = \cos(\theta_r/2)$ and $\beta = \sin(\theta_r/2)e^{i\phi}$ which are parameterized by the polar (Rabi) angle θ_r and the phase angle ϕ. The phase angle ϕ is expressed relative to the phase of the local oscillator used in the heterodyne detection scheme and therefore can always be chosen to be zero. We characterize the prepared qubit state using a pulsed dispersive measurement of the resonator transmission [15] and clearly observe Rabi oscillations in the qubit population $P_e = |\beta|^2$ versus the amplitude $A_r \propto \theta_r$ (Fig. 2a). After qubit state preparation, we apply a current pulse of controlled amplitude and duration to the flux bias line to tune the qubit transition frequency into resonance with the resonator frequency ν_r. We time-resolve the resonant vacuum Rabi oscillations of the coupled system at a frequency of $2g/(2\pi) = 118$ MHz by dispersively measuring the qubit state after it has been tuned back to the frequency ν_q strongly detuned from the resonator (Fig. 2b). Adjusting the qubit-resonator interaction time to half a vacuum Rabi period $t_{vr} = \pi/g = 4.2$ ns, we coherently map the qubit state $|\psi_q\rangle$ to an equivalent superposition state $|\psi_c\rangle = \alpha|0\rangle + \beta|1\rangle$ of the $|0\rangle$ and $|1\rangle$ photon Fock states stored in the resonator mode a, while the qubit returns to the ground state. Similar techniques have been used to prepare and measure a wide range of intra-cavity photon superposition states in recent experiments both with superconducting circuits [16] and with Rydberg atoms [17]. It is important to note that this technique relies on a reliable preparation of the vacuum state in the resonator prior to the controlled vacuum Rabi oscillations. The choice of the interaction time t_{vr} is based on the assumption that the coupled system carries maximally one excitation for which the vacuum Rabi frequency is $2g/(2\pi)$. If the resonator is in a weak thermal state the final state will not be $|\psi_c\rangle$ but generally an entangled state between qubit and resonator as discussed at the end of this report.

In the following we discuss the characterization of the photon states in the cavity by measuring the quadrature amplitudes of the microwave fields emitted from *both* ends of the cavity, see schematic in Fig. 1b. For this purpose we have realized a symmetric circuit QED setup in which the output fields are detected independently and simultaneously at both ports of the cavity. Our

scheme comprises two independent detection chains similar to the one pioneered by Gabelli *et al.* [9]. Each chain consists of a cold amplifier with gain $G_{b,c} \approx 33 \, \mathrm{dB}$ and noise temperature $T_{\mathrm{N}(b,c)} \approx 4.5 \, \mathrm{K}$ followed by a two stage heterodyne detector in which the signal is down converted from the resonator frequency to $25 \, \mathrm{MHz}$ in an analog stage and to d.c. in a digital homodyne stage. This allows measurement of the electric field at both ends of the resonator characterizing the radiation emitted into the modes labeled b and c. In this way, we extract the complex envelope [18] $S_{b,c}(t)$ of the amplified electric field $E_{b,c}^{(+)}$ described by

$$E_{b,c}^{(+)}(t) + N_{b,c}(t) = S_{b,c}(t)e^{-2\pi i \nu_{\mathrm{r}} t} \tag{1}$$

where the real and imaginary part of $S_{b,c}(t)$ are the two field quadratures in the frame rotating at the resonator frequency and $N_{b,c}(t)$ is the noise added by the amplifier. Using input-output theory [19], one can show that the full information about the intra-cavity mode a can be extracted from a measurement of the propagating modes b and c [20]. It is interesting to note that our setup is essentially equivalent to one in which the radiation emitted by a source is investigated at the two output ports of a beam splitter [20]. Considering the expressions for all field operators in the Heisenberg picture we find a formal equivalence, where the resonator mode a is equivalent to the beam splitter input mode. Furthermore, the modes b and c are equivalent to the beam splitter output modes and the cavity input modes are equivalent to the vacuum port of the beam splitter. This allows us to realize a Mach-Zehnder interferometer or a Hanbury Brown-Twiss type setup to investigate the radiation in the mode a without explicitly implementing a microwave beam splitter.

As a first step, we characterize zero and one photon superposition states by measuring the time dependence of the average quadrature amplitudes of the electric field of the output mode b at one end of the resonator. This gives us access to the expectation value of the annihilation operator of the cavity field $\langle S_b(t) \rangle \propto \langle a(t) \rangle$ [20]. Similar measurements were presented in Ref. [5], where the cavity photon was created by Purcell limited spontaneous emission. Figure 3a shows the real part of $\langle S_b(t) \rangle$ versus time t after the preparation of the photon superposition state $|\psi_{\mathrm{c}}\rangle$ characterized by the qubit Rabi angle θ_r used for its preparation. We find excellent agreement with the expected average field quadrature amplitude $\langle a \rangle \propto \sin(\theta_r)/2$ (Fig. 3c), where we get the largest signals for the superposition states $|\psi_{\mathrm{c}}^+\rangle = (|0\rangle + |1\rangle)/\sqrt{2}$ and $|\psi_{\mathrm{c}}^-\rangle = (|0\rangle - |1\rangle)/\sqrt{2}$ prepared using $\theta_r = \pi/2$ and $3\pi/2$, respectively. As expected from the uncertainty principle, the Fock states $|0\rangle$ and $|1\rangle$ prepared with $\theta_r = 0$ and π, respectively, do not show any quadrature amplitude signals (Fig. 3a) since their phase is completely uncertain. For all of the above measurements, the overall global phase of the signals is adjusted such that the imaginary part of $\langle S_b(t) \rangle$ is equal to zero which therefore is not displayed. We also note that the amplifier noise averages to zero in the quadrature amplitude measurement. Moreover, the time dependence of all measurement traces is well understood. For the state $|\psi_{\mathrm{c}}^+\rangle$ (Fig. 3b), for example, the characteristic decay time is given by twice the cavity decay time $2T_\kappa = Q/\pi\nu_r = 102 \, \mathrm{ns}$. The rise time, which should ideally be $t_{\mathrm{vr}} = 4.2 \, \mathrm{ns}$, is limited by the bandwidth $BW = 15 \, \mathrm{MHz}$ of our detection scheme.

In our measurement scheme, we simultaneously record the time dependent quadrature amplitudes $S_{b,c}(t)$ detected at both ports of the cavity for *each* single photon that we generate. This is realized using a two channel analog-to-digital converter (ADC) with a time resolution of $10 \, \mathrm{ns}$. Based on the measurement record of each event, we can then calculate *any* expectation value, such as averages, products or correlations, that can be expressed in terms of the detected output signals $S_{b,c}(t)$. Processing this data in real time using field programmable gate array (FPGA) electronics allows us to efficiently extract information even in the presence of substantial noise added by the amplifier.

As a first experiment taking advantage of this scheme, we have measured the expectation value of the instantaneous power $\langle S_b^*(t)S_b(t) \rangle$ emitted into the output mode b with the cavity
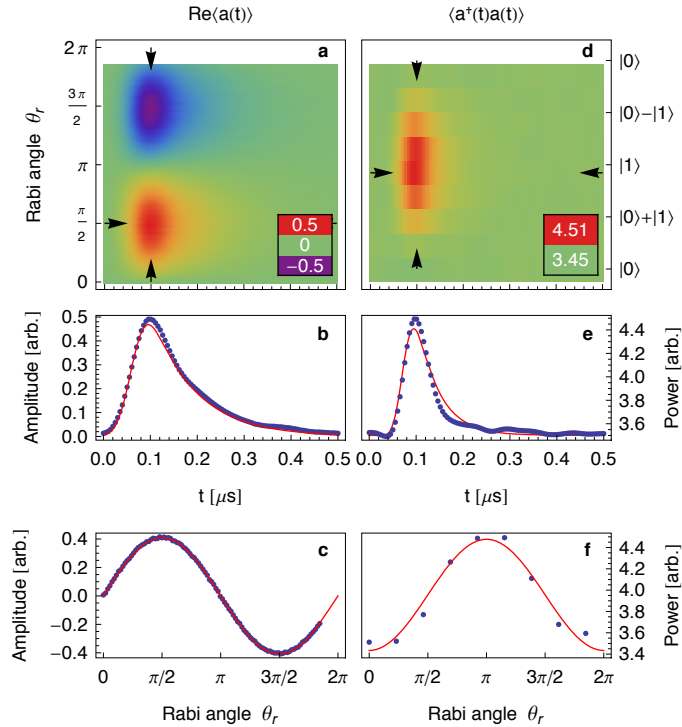
Figure 3. Quadrature amplitude and cross-power measurements. a, Measured time dependence of cavity field quadrature amplitude of mode b for zero and one photon superposition states characterized by the Rabi angle θ_r (left axis) and generated state (right axis). **b,** Single quadrature trace at $\theta_r = \pi/2$ in **a** corresponding to $(|0\rangle + |1\rangle)/\sqrt{2}$. **c,** Dependence of maximum quadrature amplitude on θ_r. **d,** Measured time dependence of cross-power between modes b and c for the same preparation as in **a**. **e,** Single power trace at $\theta_r = \pi$ in **c** corresponding to $|1\rangle$. **f,** Dependence of maximum cross-power on θ_r. Dots are data and lines are theory, see text.

mode a prepared in the Fock state $|1\rangle$ (not shown). It is important to note that we have digitally calculated the power by multiplying the quadrature amplitudes $S_b(t)$ for each single photon pulse instead of using a diode as a power meter in which the detection and the averaging is realized within the detector [5]. In this power measurement, the detected noise power of the amplifier dominates by a factor of about 1600 over the single photon power which is still observed using sufficient averaging (similar to that in Fig. 3e). By identifying the measured single photon pulse with the energy $h\nu_r$ we can compare the measured average power $\bar{P}$ to the power of the noise background $\bar{P}(N_b)$ to determine the system noise temperature as

$$T_{\mathrm{N(sys)}} \approx \frac{h\nu_r}{k_B} \cdot \frac{\eta_{\mathrm{filter}}}{BW t_p} \cdot \frac{1}{2} \frac{\bar{P}(N_b)}{\bar{P} - \bar{P}(N_b)} \approx 25\,\mathrm{K}, \tag{2}$$

with Planck constant h, Boltzmann constant k_B, and the time between photon preparations $t_p = 512\,\mathrm{ns}$. Finally we account for the fact that the finite bandwidth of the detection chain filters out a part of the single photon pulse by introducing the efficiency $\eta_{\mathrm{filter}} = 0.78$ given by the overlap of the photon spectrum and the detection bandwidth. The factor $1/2$ reflects the fact that we only detect half of all emitted photons on one side of the cavity. We find that $T_{\mathrm{N(sys)}}$ is substantially higher than the noise temperature of the amplifiers because of absorption in the cables and insertion loss of components in the detection chain.

Calculating the cross-power $\langle S_b^*(t) S_c(t) \rangle$ between the two output modes instead of the direct power emitted into just a single output mode, we can reject most of the noise added by the amplifiers, demonstrating the versatility of our digital scheme. The detected cross-power is related to the average photon number in the cavity as [20]

$$\langle S_b^*(t) S_c(t) \rangle \propto \langle a^\dagger(t) a(t) \rangle + P(N_{bc}), \tag{3}$$

where $P(N_{bc})$ is the power of correlated noise between channels b and c. In these measurements, the detected noise cross-power is significantly smaller than the direct noise power of each

amplifier as the two detection chains add predominantly uncorrelated noise. The equivalent temperature of the residual correlations is found to be $520\,\text{mK}$ in these particular measurements, which can only be partly explained by the physical temperature of the sample. Therefore we conclude that a substantial part of these residual correlations are of technical origin, such as insufficient isolation of the two amplifier chains, correlated digitizer noise and residual resonator thermal noise due to incomplete thermalization of the resonator inputs. In more recent measurements where we use a similar two channel detection setup with improved thermalization and better insolation we find correlated noise with an equivalent temperature of about $80\,\text{mK}$ which corresponds to a correlated noise power much smaller than the output power of the single photon source.

We have characterized the measured cross-power of our single photon source for the same set of cavity superposition states as used for the quadrature amplitude measurements (Fig. 3d). We find excellent agreement of the temporal evolution of the cavity photon number in dependence on the preparation angle of the photon state $\langle a^\dagger a \rangle \propto \sin^2(\theta_r/2)$ (Fig. 3f). The maximum cross-power is measured for the Fock state $|1\rangle$ ($\theta_r = \pi$) and the minimum power for the $|0\rangle$ state ($\theta_r = 0$ or 2π) (Fig. 3d).

Finally, we have characterized our single photon source using time-dependent first-order cross-correlation measurements of the two output modes of the resonator

$$\Gamma^{(1)}(\tau) = \int \langle S_b^*(t) S_c(t+\tau) \rangle dt \,. \tag{4}$$

For this purpose, we generate a train of 40 single photon pulses, each created using the procedure described above, with a pulse separation of $t_{\text{p}} = 512\,\text{ns}$ which is much greater than the qubit and cavity decay times. To remove the background of the correlated noise, we subtract the measured correlation function $\Gamma_{ss}^{(1)}(\tau)$ in the resonator steady-state from the signal acquired when performing the photon state preparation sequence $\Gamma^{(1)}(\tau)$. From the recorded quadrature amplitude data, we calculate in real-time

$$\Gamma^{(1)}(\tau) - \Gamma_{ss}^{(1)}(\tau) \propto G^{(1)}(\tau) \,, \tag{5}$$

which gives us access to the first-order correlation function $G^{(1)}(\tau) = \int \langle a^\dagger(t) a(t+\tau) \rangle dt$ of the resonator field [20]. To measure each trace in Fig. 4a, 128×10^6 trains of 40 photons were prepared in a specific state and $G^{(1)}(\tau)$ was calculated in real time using our FPGA based electronics, corresponding to more than 1 terabyte of data that have been evaluated in approximately 1 hour.

The correlation function data $G^{(1)}(\tau)$ (Fig. 4a) is characterized by a set of peaks that are separated by the repetition time t_{p} of the single photon source. The amplitude of $G^{(1)}$ at $\tau = 0$ and $\tau = n t_{\text{p}}$, representing the correlation between a pulse i and $i+n$, depends in a characteristic fashion on θ_{r}. For the Fock state $|1\rangle$ (at $\theta_r = \pi$), the correlation function $G^{(1)}(0)$ is at a maximum and vanishes at $G^{(1)}(n t_{\text{p}})$ as there is no coherence between photons emitted from the source at different times. In fact, $G^{(1)}(0) \propto \langle a^\dagger a \rangle \propto |\beta|^2 = \sin(\theta_r/2)^2$ oscillates sinusoidally with the preparation angle, as it essentially measures the average photon number of the generated field (Fig. 4b). For photon superposition states, the expectation values of $\langle a^\dagger \rangle$ and $\langle a \rangle$ of subsequently generated photon states have non-vanishing values, as discussed before. Since photons from different repetitions of the experiments are uncorrelated, $G^{(1)}(n t_{\text{p}}) \propto \langle a^\dagger \rangle \langle a \rangle$ which has a finite value and oscillates at half the period. Thus, $G^{(1)}(n t_{\text{p}}) \propto |\alpha\beta|^2 = \sin^2(\theta_r)/4$ is maximized for the states $|\psi_{\text{c}}^+\rangle$ and $|\psi_{\text{c}}^-\rangle$ (Fig. 4b).

The observed features of the first-order correlation function together with the results presented in Fig. 3 confirm that we have implemented a deterministic single photon source. Considering the well controlled procedure implemented for generating the single photon pulses,
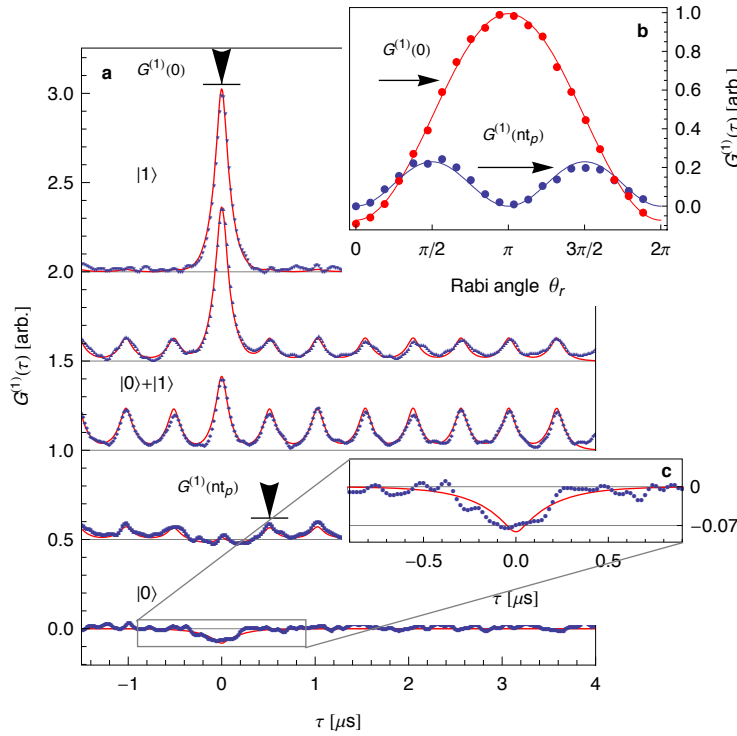
Figure 4. **Correlation function measurements. a,** Time dependence of first-order correlation function of the cavity field $G^{(1)}$ for indicated states. Data is offset for improved visibility. **b,** Correlation function at $\tau = 0$ and $\tau = nt_p$ versus θ_{r}. Dots are data, lines are predictions. **c,** Enlarged trace for $\theta_{\mathrm{r}} = 0$ from **a** displaying cavity field cooling.

any other pulsed coherent or thermal field can essentially be ruled out as being the source of the measured correlations. This indicates for our scheme that the quantum mechanical properties of the radiation are not lost in the detection chain but are fully retained in the form of statistical information of the data and can be extracted by appropriate single-shot analysis. Measurements of the second-order correlation function $G^{(2)}$ provide unambiguous proof of the quantum character of the field, independent of any prior knowledge about its source [1, 12].

Interestingly, our time-dependent first-order correlation function measurements allow us to observe cooling of the resonator field through its interaction with the qubit in its ground state. If the thermal occupation of the qubit excited state is substantially smaller than the thermal occupation of the resonator, the qubit can absorb a photon from the resonator during the interaction time t_{vr}. The qubit then emits the photon into the environment at a different frequency thereby cooling the resonator field. If we take the theoretical values for $G^{(1)}$ and correct them to first order for a small thermal state in the resonator with mean photon number $n_{\mathrm{bg}} \ll 1$ during the state preparation, we find for the first-order correlation measurements with background subtraction

$$G^{(1)}(nt_{\mathrm{p}}) \propto (\sin^2(\theta_r)/4)(1 - n_{\mathrm{bg}}(1 + \cos\sqrt{2}\pi))^2 \tag{6}$$

$$G^{(1)}(0) \propto \sin(\theta_r/2)^2(1 + n_{\mathrm{bg}}\sin^2\sqrt{2}\pi) - n_{\mathrm{bg}}. \tag{7}$$

where the factors $\sqrt{2}$ indicate the faster vacuum Rabi oscillation of two excitations in the system. When we try to prepare the vacuum state in the cavity ($\theta_{\mathrm{r}} = 0$), the value of $G^{(1)}(0) = -n_{\mathrm{bg}}$ is a direct measure of the background field photon number which is cooled by the qubit interaction. In our measurement in Fig. 4c this is observable as a pronounced dip in the measured $G^{(1)}(\tau)$ around $\tau = 0$, which allows us to extract the thermal background population of the resonator $n_{\mathrm{bg}} = 0.07$ corresponding to a field temperature of $T_{\mathrm{bg}} = 115\,\mathrm{mK}$. This temperature is in good agreement with independent measurements of T_{bg} from the vacuum Rabi mode splitting spectrum [21]. Analyzing the time dependent correlation function measurements in the presence

of a weak thermal background field, we find excellent agreement between our data and Eq. (6) for all prepared field states (see solid lines in Fig. 4).

Our experiments clearly demonstrate that correlation function measurements based on quadrature amplitude measurements can be used to characterize quantum properties of propagating microwave frequency radiation fields. Even in the presence of noise added by the amplifier, efficient data processing techniques and two channel detection allow measurements of higher statistical moments of the fields. We have also demonstrated that the cavity field can equivalently be characterized measuring both cavity outputs using a two channel detection method instead of using a beam splitter. When better, possibly quantum limited, amplifiers [22] become available the demonstrated techniques may also help to enable the full tomography of propagating radiation fields. Furthermore, the flexibility of circuit design and the high level of control achievable in circuit QED will enable a variety of future experiments with quantum microwave fields for basic research and applications.

References
 [1] Walls D and Milburn G 1994 *Quantum Optics* (Berlin: Springer Verlag)
 [2] Glauber R J 1963 *Phys. Rev.* **130** 2529–2539
 [3] Glauber R J 1963 *Phys. Rev. Lett.* **10** 84–86
 [4] Brown R H and Twiss R Q 1957 *Proc. R. Soc. (London) A* **242** 300–324
 [5] Houck A, Schuster D, Gambetta J, Schreier J, Johnson B, Chow J, Frunzio L, Majer J, Devoret M, Girvin S and Schoelkopf R 2007 *Nature* **449** 328–331
 [6] Caves C M 1982 *Phys. Rev. D* **26** 1817–1839
 [7] Grosse N B, Symul T, Stobinska M, Ralph T C and Lam P K 2007 *Phys. Rev. Lett.* **98** 153603
 [8] Pozar D M 1993 *Microwave Engineering* (Addison-Wesley Publishing Company)
 [9] Gabelli J, Reydellet L H, Feve G, Berroir J M, Placais B, Roche P and Glattli D C 2004 *Phys. Rev. Lett.* **93** 056801
[10] Mariantoni M, Menzel E P, Deppe F, Araque Caballero M A, Baust A, Niemczyk T, Hoffmann E, Solano E, Marx A and Gross R 2010 *Phys. Rev. Lett.* **105** 133601
[11] Menzel E P, Deppe F, Mariantoni M, Araque Caballero M A, Baust A, Niemczyk T, Hoffmann E, Marx A, Solano E and Gross R 2010 *Phys. Rev. Lett.* **105** 100401
[12] Bozyigit D, Lang C, Steffen L, Fink J M, Eichler C, Baur M, Bianchetti R, Leek P J, Filipp S, da Silva M P, Blais A and Wallraff A 2010 *Nat. Phys.*, in press
[13] Koch J, Yu T M, Gambetta J, Houck A A, Schuster D I, Majer J, Blais A, Devoret M H, Girvin S M and Schoelkopf R J 2007 *Phys. Rev. A* **76** 042319
[14] Wallraff A, Schuster D I, Blais A, Frunzio L, Huang R S, Majer J, Kumar S, Girvin S M and Schoelkopf R J 2004 *Nature* **431** 162–167
[15] Bianchetti R, Filipp S, Baur M, Fink J M, Göppl M, Leek P J, Steffen L, Blais A and Wallraff A 2009 *Phys. Rev. A* **80** 043840
[16] Hofheinz M, Wang H, Ansmann M, Bialczak R C, Lucero E, Neeley M, O'Connell A D, Sank D, Wenner J, Martinis J M and Cleland A N 2009 *Nature* **459** 546–549
[17] Deleglise S, Dotsenko I, Sayrin C, Bernu J, Brune M, Raimond J M and Haroche S 2008 *Nature* **455** 510–514
[18] Mandel L and Wolf E 1995 *Optical Coherence and Quantum Optics* (Cambridge University Press)
[19] Gardiner C W and Collett M J 1985 *Phys. Rev. A* **31** 3761–3774
[20] da Silva M P, Bozyigit D, Wallraff A and Blais A 2010 *Phys. Rev. A* **82** 043804
[21] Fink J M, Baur M, Bianchetti R, Filipp S, Göppl M, Leek P J, Steffen L, Blais A and Wallraff A 2009 *Phys. Scr.* **T137** 014013
[22] Castellanos-Beltran M A, Irwin K D, Hilton G C, Vale L R and Lehnert K W 2008 *Nat. Phys.* **4** 929–931